Equilibrating Temperaturelike Variables in Jammed Granular Subsystems

James G. Puckett and Karen E. Daniels

Department of Physics, North Carolina State University, Raleigh, North Carolina 27695, USA

(Received 31 July 2012; published 31 January 2013)

Although jammed granular systems are athermal, several thermodynamiclike descriptions have been proposed which make quantitative predictions about the distribution of volume and stress within a system and provide a corresponding temperaturelike variable. We perform experiments with an apparatus designed to generate a large number of independent, jammed, two-dimensional configurations. Each configuration consists of a single layer of photoelastic disks supported by a gentle layer of air. New configurations are generated by cyclically dilating, mixing, and then recompacting the system through a series of boundary displacements. Within each configuration, a bath of particles surrounds a smaller subsystem of particles with a different interparticle friction coefficient than the bath. The use of photoelastic particles permits us to find all particle positions as well as the vector forces at each interparticle contact. By comparing the temperaturelike quantities in both systems, we find compactivity (conjugate to the volume) does not equilibrate between the systems, while the angoricity (conjugate to the stress) does. Both independent components of the angoricity are linearly dependent on the hydrostatic pressure, in agreement with predictions of the stress ensemble.

DOI: 10.1103/PhysRevLett.110.058001 PACS numbers: 45.70.Cc, 81.05.Rm

Granular materials are a collection of discrete, athermal particles. In the absence of an external driving force, these materials relax into a mechanically stable jammed state and cannot move into another configuration since thermal fluctuations are negligible [1]. While these materials are therefore inherently nonequilibrium, preparing a configuration with a strict protocol nonetheless yields different microscopic states with the same, reproducible volume [2]. Edwards proposed that the system volume (a conserved quantity) could be used to write a granular density of states, a corresponding entropy, and a temperaturelike variable conjugate to the volume [3]. However, a complete granular statistical mechanics should describe the distribution of contact forces as well as the volumes. Subsequent theoretical advances have proposed that a stress-based ensemble [4–11] is likely required for a full treatment.

In the Edwards ensemble, the volume V plays a role analogous to that of energy in equilibrium statistical mechanics. A granular temperature, dubbed the compactivity, is defined as $X \equiv (\partial S/\partial V)^{-1}$, and has been successfully measured in models [12,13], simulations [14,15], and experiments [16–21]. Similarly, the stress ensemble considers force and torque constraints on individual particles, and writes the density of states as a function of the stress tensor $\hat{\Sigma} = \sum \vec{r}_{ij}\vec{f}_{ij}$, where the $\vec{r}_{ij}$ are the vectors pointing from the center of each particle to its contacts, and $\vec{f}_{ij}$ is the corresponding contact force. The conjugate variable is then a tensorial temperature known as the angoricity, and is defined to be $\hat{A} = (\partial S/\partial \hat{\Sigma})^{-1}$.

A minimal test of such temperaturelike variables, which are not guaranteed to be well defined in an inherently nonequilibrium system, is to consider whether they obey the zeroth law of thermodynamics. In experiments and simulations, the compactivity [20] has previously been shown to be equal in different parts of the same packing, and in different packings generated with the same particles under identical conditions. Simulations show this is also satisfied by the angoricity [7,8]. However, no test has been made of whether two dissimilar systems can equilibrate either X or $\hat{A}$. We provide such a test in a real granular system subject to isotropic compression, and find that while the compactivity fails this simple test, the angoricity equilibrates in a temperaturelike way.

Our experiments are conducted on a bidisperse granular monolayer of photoelastic disks resting on a nearly frictionless surface provided by a thin layer of pressurized air. The assembly of particles is composed of an inner subsystem and a larger bath which differ only in the interparticle friction coefficient (see Fig. 1). Starting from a dilute state, the monolayer is biaxially compressed by outer walls in a series of short steps. At some global volume fraction Φ, the system jams and for all further steps the pressure on the system increases. Finally, the walls redilate to permit large scale rearrangements before the next series begins. By repeating this protocol many times, we generate an ensemble of configurations for which we record particle positions to find local volumes and use photoelastic analysis to calculate contact forces using methods similar to [22,23]. With this information, we calculate the compactivity and angoricity for both the bath and the inner subsystem.

In the Edwards ensemble [3], assuming equiprobability and the entropy maximization principle, the probability of finding a system with volume V and compactivity X to be given by a Boltzmann-like distribution

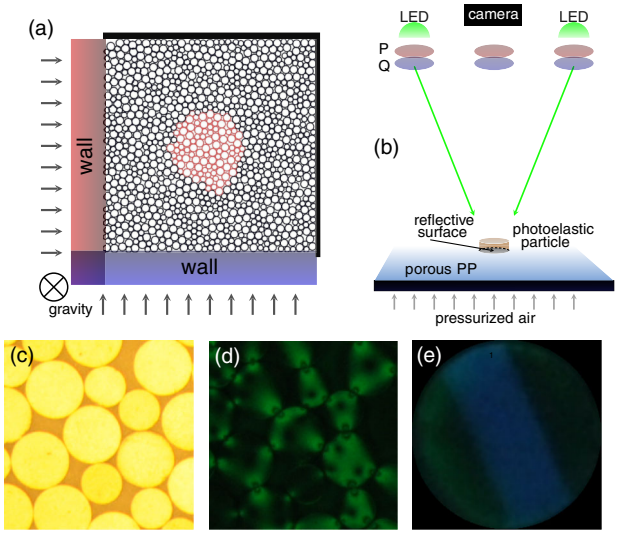

FIG. 1 (color online). Schematic of apparatus showing (a) two walls biaxially compressing an array of disk-shaped particles composed of an outer subsystem (black, high μ) and an inner subsystem (red, low μ) and (b) reflective photoelasticity on air-floated particles. Light shines from green LEDs through a linear polarizer (P) a wavelength-matched quarter wave plate (Q) before entering the photoelastic material. A mirrored surface on the bottom of each particle reflects light back through the particle. A second quarter-wave plate and linear polarizer are mounted on the camera to resolve the photoelasticity. Three images of each configuration are recorded: (c) unpolarized white light for locating particle positions, (d) polarized green light showing isochromatic fringes for calculating contact forces, and (e) an ultraviolet light for identifying the low-μ particles.

$$\mathcal{P}(V) = \frac{\Omega(V)}{Z(X)} e^{-V/X}, \tag{1}$$

where the density of states is $\Omega(V)$ is defined for an ensemble of jammed configurations, and the partition function is $Z(X)$. As originally proposed by Edwards, the volume V referred to the *global* volume of the system, which exchanged volume with its surroundings. Recently, attention has focused on the *local* (particle-scale, Voronoï) volumes, which exchange volume with other parts of the same system [20,24]; this local ensemble will be the focus of our investigations. The stress ensemble, using conservation of the local force-moment tensor $\hat{\Sigma}$, similarly proposes a local Boltzmann-like distribution

$$\mathcal{P}(\hat{\Sigma}) = \frac{\Omega(\hat{\Sigma})}{Z(\hat{A})} e^{-\mathrm{Tr}(\hat{\Sigma}/\hat{A})}, \tag{2}$$

where the angoricity $\hat{A}$ is a tensor. The temperaturelike variables X and $\hat{A}$ describe the size of the fluctuations of V and $\hat{\Sigma}$, respectively.

To calculate either X or $\hat{A}$, we use two methods: the method of overlapping histograms [7,20,25] and the fluctuation-dissipation theorem (FDT) [16,17,21]. The ratio of $\mathcal{P}(V)$ between two systems is exponential in V and is given by

$$\frac{\mathcal{P}_1(V)}{\mathcal{P}_2(V)} = \frac{Z(X_2)}{Z(X_1)} e^{(1/X_2 - 1/X_1)V}. \tag{3}$$

By taking the logarithm of this ratio, one obtains a term linear in V, where the coefficient is the difference in the inverse temperatures. The success of using this approach supports the assumptions of the Edwards ensemble and the Boltzmann-like distribution of V [20]. This method determines $1/X$ up to an additive constant: $1/X \to 1/X + C_X$. The FDT method also provides a relative measurement. Using the measured variance $\langle \delta V^2 \rangle$ of $\mathcal{P}(V)$, we compute

$$\frac{1}{X_1} - \frac{1}{X_2} = \int_{V_1}^{V_2} \frac{dV}{\langle \delta V^2 \rangle} \tag{4}$$

to obtain values of X, also up to a constant. The calculation of $\hat{A}$ utilizes equations analogous to Eqs. (3) and (4); the tensorial aspects will be discussed in more detail below. Each of these methods is used separately on both the subsystem and the bath, in order to test for equilibration.

Our experimental apparatus is shown to scale in Fig. 1. The granular monolayer consists of 1004 bidisperse photoelastic (Vishay PhotoStress PSM-4) disks with a thickness ≈ 3.1 mm and diameters $d_S = 11.0$ mm and $d_L = 15.4$ mm, in equal concentrations. The particles are supported on a thin layer of air provided by a steady flow of pressurized air through a porous polypropylene sheet with a nominal pore size of 120 μm. This minimizes the effect of friction between the particles and the surface, but does not otherwise cause significant dynamics once the system is jammed. The sheet is leveled (particles do not drift to one side) and flat (particles do not cluster). The system consists of an outer bath $N_B = 904$ and an inner subsystem $N_S = 100$. Particles in the bath have a friction coefficient $\mu_B \approx 0.8$, while particles in the inner subsystem are wrapped with a thin layer of polytetrafluoroethylene (Teflon) tape with a $\mu_S < 0.1$.

Images of the particle positions, photoelastic images for measuring vector contact forces, and identification of the subsystem particles are recorded with three separate images captured by a single CCD camera located above the apparatus [see Fig. 1(b)]. Particle positions are identified using a white light image [see Fig. 1(c)], from which the centers are detected with an accuracy of $\approx 0.01 d_S$ using a Hough transform. The photoelastic images [see Fig. 1(d)] are captured using reflective photoelasticity, in which the silvered back side of each particle reflects polarized light back to the camera. Photoelasticity allows for the numerical determination of the normal and tangential forces at each contact point, as required to measure $\hat{\Sigma}$. Similar to the methods pioneered by [22,23], we minimize the error between the observed and fitted image of the particle using a nonlinear least-squares optimization. Details and source code are available for download at [26]. The third image is

taken using black-light illumination to identify the subsystem particles, which are tagged with ultraviolet-sensitive ink [see Fig. 1(e)]. The subsystem comprises all low-μ particles which are Voronoï neighbors with at least one other particle in the subsystem.

The particles are confined within a square region (maximally 50×50 cm) imposed by two stationary walls positioned by stepper motors, as shown in Fig. 1(a). The system is initially in a dilute, well-mixed, unjammed state, with the global volume fraction $\Phi \lesssim 0.6$. The two walls biaxially compress the system by a series of small steps of constant size ($\Delta\Phi = 0.0009$, equivalently $\Delta x = 0.3$ mm or $0.02 r_L$). With each step of the wall, the three images are recorded, and data are collected over a series of volumes corresponding to $0.775 < \Phi < 0.805$, giving 30 different volumes for each compression cycle. Steps continue until the gradient squared of the force image [27] indicates a pressure threshold has been reached; this reduces the risk of particles buckling out of plane. The walls then redilate to the dilute state, and the particles are then mixed while maintaining subsystem continuity; this protocol is repeated 100 times.

During the compression phase of each quasistatic cycle, we observe the percolation of force chains throughout both the bath and the subsystem at a value Φ_{perc}. As the system is further compressed beyond this point, the contact forces grow in strength and the average number of contacts per particle increases. For the set of 100 cycles, this threshold occurs over a range $0.782 < \Phi_{\text{perc}} < 0.792$, where the width of the distribution is indicative of finite size effects [28,29]. The ratio of unjammed to jammed systems at a given Φ is shown in Fig. 2(d). We define random loose packing as $\Phi_{\text{RLP}} = \langle \Phi_{\text{perc}} \rangle \approx 0.787$ as the center of this distribution.

We calculate the distribution of local volumes $\mathcal{P}(V_m)$ over clusters of size m, using the sum of individual radical Voronoï volumes obtained from the Voro++ software [30]. Each cluster is defined as the $m-1$ nearest neighbors surrounding a central particle. For $m = 1$, $\mathcal{P}(V_m)$ has two distinct peaks which correspond to small and large particles [18]. With increasing cluster size, the bimodal aspect of $\mathcal{P}(V_m)$ disappears, but even for large cluster sizes ($m > 100$), the distribution remains asymmetric and non-Gaussian [18]. In Fig. 2(a), we show $\mathcal{P}(V_m)$ for three values of Φ with $m = 48$; the value of m is large enough so that $\mathcal{P}(V_m)$ does not show any features arising from bidispersity.

In Fig. 2(b), we show the ratio $\mathcal{P}_i(V)/\mathcal{P}_j(V)$ where the reference system j is $\Phi = 0.784$. In practice this can be done with any two systems so long as there is sufficient overlap between their histograms. As the ratio of $\mathcal{P}_i(V)/\mathcal{P}_j(V)$ is well approximated by an exponential in V, the compactivity can be calculated using Eq. (3). The inverse compactivity $1/X$ is also calculated using FDT using Eq. (4), where the integrand is approximated using

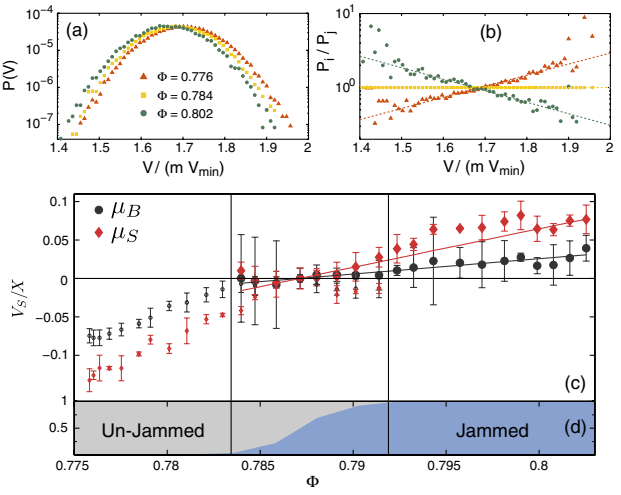

FIG. 2 (color online). (a) Volume histograms $\mathcal{P}(V)$ for $\Phi = 0.776$ (filled upward triangle), 0.784 (filled square), and 0.802 (filled circle) with $m = 48$. (b) A semilogarithmic plot of the ratio each histogram with respect to the $\Phi = 0.784$ distribution, i.e., $\mathcal{P}_i(V)/\mathcal{P}_{i=2}(V)$. (c) The inverse compactivity given by Eq. (3) plotted as a function of the inverse volume fraction where μ_B are shown as black filled circle and μ_S are red filled diamond. Large (small) symbols denote jammed (unjammed) configurations, respectively. Error bars shown are uncertainties in $\mathcal{P}(V)$ and propagated through the calculation. The inverse compactivity given by the FDT method [Eq. (4)], is shown with the solid line for comparison. (d) The ratio of the number of jammed (unjammed) configurations recorded at each Φ.

a third order polynomial. Each method determines $1/X$ only up to an additive constant, which is adjusted so that $X_{\text{RLP}} = \infty$. In Fig. 2(c), the inverse compactivity is shown for both the bath ($1/X_B$) and the subsystem ($1/X_S$). We find good agreement between $X(\Phi)$ given by the overlapping histogram method and by the fluctuation dissipation theorem. In addition, for $4 < m < 50$, we observe X to be approximately independent of m. However, we find that the compactivity of the bath is not equal to that of the subsystem [$X_B(\Phi) \neq X_S(\Phi)$]. Because the slopes of the two curves differ, this observation cannot be accounted for by adjusting the additive constant (effectively, adjusting Φ_{RLP}) for the two particle types. This represents a failure of the zeroth law for X. However, it is possible that equilibration would occur under alternative preparation protocols, for instance those in which particle rearrangements were more prevalent (e.g., tapping or shearing).

We can take further advantage of the accessibility of both jammed and unjammed states within in the center of the range of explored Φ. While the Edwards ensemble is not defined for unjammed systems, we can, nonetheless, carry out the histogram analysis as performed on the jammed systems. In this regime, we find that the $\mathcal{P}(V_m)$ histograms cannot distinguish between the jammed and unjammed states. Furthermore, the measured values of X decrease continuously from above Φ_{RLP} to below; this is an undesirable characteristic.

The stress ensemble also provides a Boltzmann-like distribution in the stress, as given in Eq. (2). In the case of frictionless grains, the angoricity $\hat{A}$ is a scalar due to the off-diagonal components in $\hat{\Sigma}$ being zero. In any real granular system, friction is present and a shear-free state is not readily obtained. Therefore, $\hat{\Sigma}$ is a symmetric tensor with nonzero off-diagonal components and can be reduced to two independent components related to the pressure and shear stress. The pressure angoricity A_p and the shear angoricity A_τ are conjugate to $\sigma_p = (\sigma_1 + \sigma_2)/2$ and the $\sigma_\tau = (\sigma_1 - \sigma_2)/2$, respectively [8], where $\sigma_{1,2}$ are the principal stresses. The average hydrostatic pressure per particle in the system is given by $\Gamma = \mathrm{Tr}\hat{\Sigma}/N$. Both A_p and A_τ are obtained using the method of overlapping histograms [analogous to Eq. (3)] and the FDT [analogous to Eq. (4)]. With each method, A is calculated up to an additive constant so that $1/A \to 1/A + C_A$, where C_A satisfies $A \to \infty$ as $\Gamma \to \infty$.

In Fig. 3(a), the local distribution of pressure $\mathcal{P}(\sigma_p)$ is shown for $m = 8$ on configurations over a range $0.0006 < \Gamma < 0.0025$ N m. The ratio $\mathcal{P}_i(\sigma_p)/\mathcal{P}_j(\sigma_p)$ is exponential in σ_p [see Fig. 3(b), similar results for σ_τ not shown], as required by the stress ensemble analogue of Eq. (3). In addition, we observe that the variance of σ_p is proportional to m, which is consistent with S being an extensive entropy

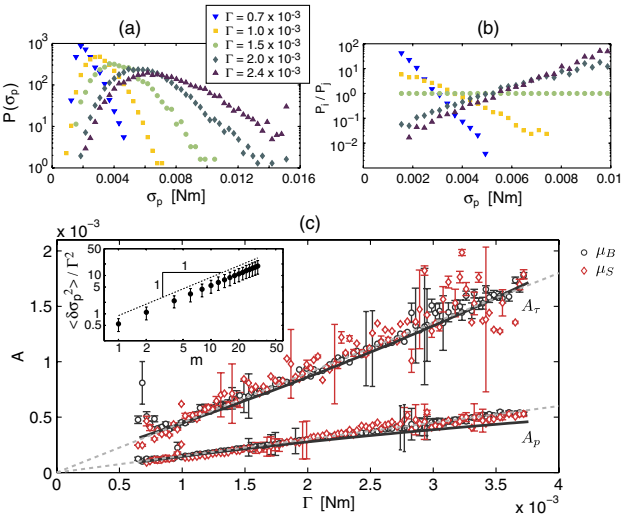

FIG. 3 (color online). (a) Distribution of σ_p where $m = 8$ and $\Gamma = 0.0007$ (filled downward triangle), 0.0010 (filled square), 0.0015 (filled circle), 0.0020 (filled diamond), and 0.0024 N m (filled upward triangle). A semilogarithmic plot of the (b) ratio $\mathcal{P}_i(\sigma_p)/\mathcal{P}_j(\sigma_p)$ where the reference system j is $\Gamma = 0.0015$ N m. The pressure angoricity A_P and shear angoricity A_τ are shown as a function of Γ where the results using overlapping histograms for μ_B and μ_S are shown as black open circle and are red open triangle, respectively. The solid line is the angoricity calculated using FDT. The gray dashed lines provide a visual reference of the slopes 0.15 and 0.45, respectively. Inset: The scaled variance $\langle \delta\sigma_p^2 \rangle$ of the $\mathcal{P}_j(\sigma_p)$ distribution, as a function of the cluster size m.

[see Fig. 3(c)]. We are therefore able to measure both the pressure angoricity A_p and the shear angoricity A_τ using their corresponding distributions, shown in Fig. 3(c) as a function of Γ. We find that $A_{p,\tau}$ are independent of m for $m > 3$, as also observed in simulations [7,8], and that values obtained from the histogram method (points) and the FDT method (solid line) are in approximate agreement. Finally, we find that for either the shear or compressional angoricity, the values measured in the bath and in the subsystem are equivalent, signifying the angoricity is equilibrating between the subsystems.

Nonetheless, the values of A_τ and A_p do not match each other, with the shear angoricity growing faster as a function of Γ. We find the angoricity is given by $A = b\Gamma$ for both pressure angoricity and shear angoricity, where $b_p = 0.153 \pm 0.004$ and $b_\tau = 0.450 \pm 0.020$, respectively. For a two-dimensional frictionless shear-free system, the stress ensemble predicts $b_p = 0.5$ at the isostatic point [7,8]. Above the isostatic point, the stress ensemble predicts b_p to be a function of the average contact number. The disagreement between the *frictional* and *frictionless* values of b_p implies friction significantly affects the density of states.

We have measured both compactivity X (conjugate to volume in the Edwards ensemble), and angoricity $\hat{A}$ (conjugate to the stress tensor in the stress ensemble), in a laboratory granular system using particle-scale characterizations. While we found that while the value of X calculated using the overlapping histogram method was consistent with the value found using the fluctuation-dissipation theorem, it failed to equilibrate between nonidentical systems, making it a poor state variable. A similar failure is likely behind previous measurements by Schröter *et al.* [17], in which two granular materials with different frictional properties, prepared using the same protocol, were found to have different globally measured values of X. In contrast, we observed that the temperaturelike variable $\hat{A}$ does successfully equilibrate between a subsystem and bath with dissimilar interparticle friction coefficients, as would be required in order to have a valid zeroth law. Moreover, we find agreement with the prediction that angoricity should scale linearly the hydrostatic pressure [8]. These successes make angoricity a promising state variable for frictional granular systems.

One downside to using angoricity as a state variable, particularly in experiments, is that its calculation requires the determination of both normal and tangential forces. While there has been a long history of measuring normal forces at the boundaries of granular systems [31–35], particle-scale measurements have seen more limited development. Outside of photoelastic particles such as those used here, measurements typically exist only for normal forces, whether the systems are frictional (tangential forces are neglected) [36,37] or frictionless [38–40].

It is possible to understand the success of the stress ensemble over the Edwards (volume) ensemble by

considering the underlying physics behind the conserved quantities in each. Under Newton's third law, forces and torques must be strictly balanced at each force contact, while volume is merely constrained globally. As a result, our subsystem differed from the bath not only in the measured X, but more conventionally in the mean local volume fraction.

In fact, the full canonical Edwards ensemble [6] unifies the volume and stress ensembles, where the density of states depends on both V and $\hat{\Sigma}$, and it has recently been argued [41,42] that the two should not be considered separately. The classic phenomenon of Reynolds dilatancy [43] under which shear induces a bulk expansion similarly suggests that such a coupling is important. Nonetheless, we observed here that angoricity can be independently equilibrated, and future experiments should more fully investigate the relationship between ensembles, the relative importance of shear and compression, and the role of friction on the density of states.

The authors are grateful for financial support under from the National Science Foundation (DMR-0644743), and for illuminating discussions with Dapeng Bi, Bulbul Chakraborty, Silke Henkes, Frederic Lechenault, Brian Tighe, Matthias Schröter, and Song-Chuan Zhao.

[1] H. Jaeger, S. R. Nagel, and R. P. Behringer, Rev. Mod. Phys. **68**, 1259 (1996).
[2] J. B. Knight, C. G. Fandrich, C. N. Lau, H. M. Jaeger, and S. R. Nagel, Phys. Rev. E **51**, 3957 (1995).
[3] S. F. Edwards and R. B. S. Oakeshott, Physica (Amsterdam) **157A**, 1080 (1989).
[4] R. C. Ball and R. Blumenfeld, Phys. Rev. Lett. **88**, 115505 (2002).
[5] J. Goddard, Int. J. Solids Struct. **41**, 5851 (2004).
[6] S. F. Edwards, in *Proceedings of the International Conference on Powders and Grains Stuttgart, Germany, 2005*, edited by R. Garcia-Rojo, H. J. Herrmann, and S. McNamara (A. A. Balkema Publishers, Leiden, 2005), Vol. 1, p. 3.
[7] S. Henkes, C. S. O'Hern, and B. Chakraborty, Phys. Rev. Lett. **99**, 038002 (2007).
[8] S. Henkes and B. Chakraborty, Phys. Rev. E **79**, 061301 (2009).
[9] R. Blumenfeld and S. F. Edwards, J. Phys. Chem. B **113**, 3981 (2009).
[10] G. Lois, J. Zhang, T. S. Majmudar, S. Henkes, B. Chakraborty, C. S. O'Hern, and R. P. Behringer, Phys. Rev. E **80**, 060303 (2009).
[11] B. P. Tighe and T. J. H. Vlugt, J. Stat. Mech. (2011) P04002.
[12] Y. Srebro and D. Levine, Phys. Rev. E **68**, 061301 (2003).
[13] R. K. Bowles and S. S. Ashwin, Phys. Rev. E **83**, 031302 (2011).
[14] C. Song, P. Wang, and H. A. Makse, Nature (London) **453**, 629 (2008).
[15] C. Briscoe, C. Song, P. Wang, and H. A. Makse, Phys. Rev. Lett. **101**, 188001 (2008).
[16] E. R. Nowak, J. B. Knight, E. Ben-Naim, H. M. Jaeger, and S. R. Nagel, Phys. Rev. E **57**, 1971 (1998).
[17] M. Schröter, D. I. Goldman, and H. L. Swinney, Phys. Rev. E **71**, 030301 (2005).
[18] F. Lechenault, F. D. Cruz, O. Dauchot, and E. Bertin, J. Stat. Mech. (2006) P07009.
[19] P. Ribière, P. Richard, P. Philippe, D. Bideau, and R. Delannay, Eur. Phys. J. E **22**, 249 (2007).
[20] S. McNamara, P. Richard, S. K. de Richter, G. Le Caër, and R. Delannay, Phys. Rev. E **80**, 031301 (2009).
[21] S.-C. Zhao and M. Schröter (unpublished).
[22] T. S. Majmudar, Ph.D. thesis, Duke University, 2006.
[23] T. S. Majmudar, M. Sperl, S. Luding, and R. P. Behringer, Phys. Rev. Lett. **98**, 058001 (2007).
[24] T. Aste and T. Di Matteo, Phys. Rev. E **77**, 021309 (2008).
[25] D. S. Dean and A. Lefèvre, Phys. Rev. Lett. **90**, 198301 (2003).
[26] J. G. Puckett, Photoelastic Disc Solver, http://nile.physics.ncsu.edu/pub/peDiscSolve/.
[27] D. Howell, R. P. Behringer, and C. Veje, Phys. Rev. Lett. **82**, 5241 (1999).
[28] C. S. O'Hern, L. E. Silbert, A. J. Liu, and S. R. Nagel, Phys. Rev. E **68**, 011306 (2003).
[29] T. Shen, C. S. O'Hern, and M. D. Shattuck, Phys. Rev. E **85**, 011308 (2012).
[30] C. H. Rycroft, G. S. Grest, J. W. Landry, and M. Z. Bazant, Phys. Rev. E **74**, 021306 (2006).
[31] D. M. Mueth, H. M. Jaeger, and S. R. Nagel, Phys. Rev. E **57**, 3164 (1998).
[32] G. Løvoll, K. J. Måløy, and E. G. Flekkøy, Phys. Rev. E **60**, 5872 (1999).
[33] D. L. Blair, N. W. Mueggenburg, A. H. Marshall, H. M. Jaeger, and S. R. Nagel, Phys. Rev. E **63**, 041304 (2001).
[34] H. A. Makse, D. L. Johnson, and L. M. Schwartz, Phys. Rev. Lett. **84**, 4160 (2000).
[35] E. I. Corwin, H. M. Jaeger, and S. R. Nagel, Nature (London) **435**, 1075 (2005).
[36] S. Mukhopadhyay and J. Peixinho, Phys. Rev. E **84**, 011302 (2011).
[37] M. Saadatfar, A. P. Sheppard, T. J. Senden, and A. J. Kabla, J. Mech. Phys. Solids **60**, 55 (2012).
[38] J. Brujić, S. F. Edwards, D. V. Grinev, I. Hopkinson, D. Brujić, and H. A. Makse, Faraday Discuss. **123**, 207 (2003).
[39] J. Zhou, S. Long, Q. Wang, and A. D. Dinsmore, Science **312**, 1631 (2006).
[40] K. W. Desmond, P. J. Young, D. Chen, and E. R. Weeks, arXiv:1206.0070.
[41] K. Wang, C. Song, P. Wang, and H. A. Makse, Phys. Rev. E **86**, 011305 (2012).
[42] R. Blumenfeld, J. F. Jordan, and S. F. Edwards, Phys. Rev. Lett. **109**, 238001 (2012).
[43] O. Reynolds, Philos. Mag. Ser. 5 **20**, 469 (1885).